

Electronic Supplementary Information for
Plasma-Engraved Co₃O₄ Nanorod with Enriched Oxygen Vacancy
for Efficient Electrocatalytic Ammonia Synthesis

Bingru Lan,^{‡a} Jieying Wan,^{‡a} Chuang Guan,^c Ji Yang,^{b,*} Na Yang,^e Jiageng Zheng,^a
Xiaodong Li^{*a} and Hao Zhang^{*a,d}

^a *State Key Laboratory of Clean Energy Utilization, Zhejiang University, Hangzhou 310027, China*

^b *College of Chemistry and Chemical Engineering, Xiamen University, Xiamen 361005, China*

^c *Shandong Guoshun Construction Group Co., Ltd., Jinan 250316, China*

^d *Zhejiang University Qingshanhu Energy Research Center, 311305 Hangzhou, P. R. China*

^e *School of Materials and Energy, University of Electronic Science and Technology of China, Chengdu 611731, Sichuan China*

‡ The two authors contribute equally to this work.

* Corresponding authors.

chem.yang@xmu.edu.cn (J. Yang); lixd@zju.edu.cn (X. Li); zhang_hao@zju.edu.cn (H. Zhang)

Table of contents:

- S1 Experimental methods**
 - S1.1 Chemical reagents**
 - S1.2 Catalyst preparation**
 - S1.3 Characterizations**
 - S1.4 Electrochemical methods**
- S2 Computational methods**
- S3 Supplementary figures**
- S4 Reference**

S1 Experimental methods

S1.1 Chemical reagents

Ammonium fluoride (NH_4F), and cobalt nitrate hexahydrate ($\text{Co}(\text{NO}_3)_2 \cdot 6\text{H}_2\text{O}$) were acquired from Aladdin Industrial Co. Sodium. Potassium hydroxide (KOH) and urea ($\text{CH}_4\text{N}_2\text{O}$) were obtained from Macklin Chemical Reagent Co. These reagents were utilized for catalyst preparation. Potassium nitrate (KNO_3), sulfanilamide, and sodium nitroferricyanide dihydrate, as well as N-(1-naphthyl)ethylenediamine dihydrochloride were sourced from Aladdin Industrial Co. Salicylic acid, sodium citrate, and potassium nitrite (KNO_2) were acquired from Shanghai Dibai Biotechnology Co., Ltd. Phosphoric acid (H_3PO_4), and hydrochloric acid (HCl), and were purchased from Hangzhou Chentong Biochemical Technology Co., Ltd. P-dimethylaminobenzaldehyde ($\text{C}_9\text{H}_{11}\text{NO}$) was obtained from Zhejiang University Logistics Group Science and Education Service Center., respectively. These reagents were employed in electrochemical experiments and product analysis. All reagents were used directly without further purification.

S1.2 Catalyst preparation

Preparation of Co_3O_4 . Initially, $\text{Co}(\text{NO}_3)_2 \cdot 6\text{H}_2\text{O}$ (3 mmol), NH_4F (6 mmol), and $\text{CH}_4\text{N}_2\text{O}$ (15 mmol) were dissolved in 80 ml of deionized water. After stirring continuously for 30 minutes, a piece of cut carbon paper was immersed in the solution, and then transferred to a Teflon-lined autoclave, and heated in an oven at 120 °C for 8 hours. Upon completion of the reaction, the precursor was rinsed three times with deionized water and anhydrous ethanol, followed by drying at 80 °C for 8 hours. Subsequently, the precursor was subjected to calcination in a tube furnace at 350 °C for 2 hours under Ar atmosphere to obtain Co_3O_4 .

Preparation of $V\text{-Co}_3\text{O}_4$. The above-obtained Co_3O_4 was subjected to treatment using Inductively Coupled Plasma (ICP) under vacuum conditions with a continuous injection of 50 ml min^{-1} Ar gas. The discharge power maintained was at 150 W for a duration of 4 minutes (the catalyst's placement is depicted in Fig. S1). Subsequently,

V-Co₃O₄ was obtained after the discharge process.

S1.3 Characterizations

The catalyst's phase structure was analyzed using X-ray diffraction (XRD, Rigaku Ultima IV). The morphology was observed through transmission electron microscopy (TEM, FEI Talos F200S) and scanning electron microscopy (SEM, ZEISS Gemini SEM 300). The surface composition was investigated via X-ray photoelectron spectroscopy (XPS, Thermo Scientific K-Alpha), with the relative concentration of oxygen vacancy being measured using EPR (Bruker EMXplus-6/1). Additionally, the hydrophilicity of the material before and after plasma treatment was assessed through contact angle measurements (JY-82C). The absorption spectrum was determined using an ultraviolet visible spectrophotometer (UV, Shimadzu UV-2700). Furthermore, the energy structure was analyzed via ultraviolet photoelectron spectroscopy (UPS, Thermo ESCALAB 250XI) and ultraviolet diffraction reflection spectroscopy (UV-vis-drs, Shimadzu UV3600).

S1.4 Electrochemical methods

Electrocatalytic nitrate reduction tests: The electrochemical experiments were performed using an electrochemical workstation (CH Instruments, CHI660E) and an H-cell, wherein the two chambers were separated by a proton exchange membrane (Nafion-117). A platinum foil (2 cm × 2 cm) served as the counter electrode, and Ag/AgCl was utilized as the reference electrode. A 50 ml solution of Ar-saturated 1 M KOH and 0.1 M KNO₃ was employed as both the cathode and anode reaction fluid. Cyclic voltammograms (CVs) were initially scanned 20 times at a scan rate of 50 mV s⁻¹, spanning from 0.2 to -0.98V vs. RHE. The measured current was then normalized to the geometric area (1 cm²). Subsequently, linear scanning voltammetry (LSV) was conducted at a scan rate of 10 mV s⁻¹, ranging from 0.2 to -0.98V vs. RHE. The electrochemical reactions were carried out at different potentials (-0.08, -0.18, -0.28, -0.38, -0.48, -0.58, -0.68, -0.78 V vs. RHE) for 30 minutes each. All potentials referred to RHE were calculated using the formula: $E_{\text{RHE}} = E_{\text{Ag/AgCl}} + 0.059 \cdot \text{pH} + 0.197 \text{ V}$. The

catalytic stability of V-Co₃O₄ was evaluated through 24 repeated experiments, each lasting 1 hour, at -0.08 V vs. RHE. After each test, the H-cell was immersed in deionized water for 10 minutes and washed thrice to remove unreacted and leftover precursors.

Determination of NH₃: Ammonia (NH₃) generation was quantified using the indophenol blue spectrophotometric (IBS) method. To achieve this, three solutions (designated as A, B, and C) were prepared. Solution A involved dissolving 6.404 g of sodium salicylate and 1.312 g of NaOH in 100 mL H₂O; solution B entailed dissolving 7.5 mL of sodium hypochlorite solution (6–14% active chlorine) and 3.1 g of NaOH in 100 mL H₂O; and solution C comprised dissolving 1 g of sodium nitroferricyanide dehydrate in 100 mL H₂O. For analysis, 50 μL of the post-reaction electrolyte was extracted and diluted with 1 M KOH to a final volume of 4 mL. To this, 320 μL of solution C, 2.4 mL of solution A, and 800 μL of solution B were sequentially added. After allowing this mixture to stand for 2 h under ambient conditions, its ultraviolet–visible (UV–vis) extinction spectrum was measured using a Mapada UV-3100 spectrophotometer.

The NH₃ yield was calculated using the formula: $[\text{NH}_3] \text{ yield} = [\text{NH}_3] \times V / (17 \times t \times A)$, where $[\text{NH}_3]$ represents the mass concentration, V is the volume of the cathodic reaction electrolyte, t is the reduction time, and A is the area of the working electrode. The Faradaic efficiency (FE) was determined using the formula: $\text{FE} = (n \times F \times c \times V) / (M \times Q)$, where F is the Faraday constant, n is the number of electrons transferred, c is the calculated product concentration, V is the volume of the cathodic reaction electrolyte, M is the molecular mass of the product, and Q is the total charge during electrosynthesis.

Determination of NO₂⁻: The NO₂⁻ concentration was determined using the Griess test with UV spectrophotometry. The Griess reagent was prepared by combining N-(1-naphthyl) ethylenediamine dihydrochloride (0.1 g), sulfanilamide (1.0 g), and H₃PO₄ (2.94 mL) in 50 mL H₂O. Typically, 1.0 mL of the Griess reagent was added to 1.0 mL of the electrolyte and 2.0 mL of H₂O. After being allowed to stand for 10 minutes, the NO₂⁻ concentration was measured by UV spectroscopy at a wavelength of 540 nm.

S2 Computational methods

Utilizing the projector augmented-wave (PAW) method^{1,2}, spin-polarized density functional theory (DFT) calculations were performed to conduct first-principles calculations. The exchange-correlation potential was described by the generalized gradient approximation (GGA) with the Perdew-Burke-Ernzerhof (PBE) functional, incorporating van der Waals corrections using Grimme's DFT-D3 model^{3,4}. Due to the limitations of GGA, the GGA + U method was employed in the calculations.

A non-stoichiometric (311) surface of Co_3O_4 with additional oxygens at the bottom, aimed at preventing Co atoms from being exposed with low coordination numbers, was constructed. Eight hydrogen atoms were introduced and connected with the added oxygen atoms to preserve the oxidation state of Co atoms. A vacuum region of approximately 15 Å was included to prevent interaction between adjacent images. The energy cutoff was set at 450 eV, and $U=3.0$ eV was applied to Co as the Hubbard U model. The Brillouin-zone integration was sampled with a Γ -centered Monkhorst-Pack mesh of $3 \times 2 \times 1^3$. The structures were fully relaxed until the maximum force on each atom was less than 0.02 eV/Å, and the energy convergence standard was set at 10^{-6} eV. The adsorption free energy (G_{ads}) can be defined as, $G_{\text{ads}} = G_{* + \text{mol}} - G_* - G_{\text{mol}}$, where $G_{* + \text{mol}}$ represents the free energy of the structure with the adsorbate, G_* is the free energy of a clean surface, the electronic energy was used to approximate the free energy, and G_{mol} is the energy of an adsorbate under vacuum. The Gibbs free energies of the intermediates in the nitrate reaction were calculated using the expression:

$$\Delta G = \Delta E + \Delta E_{\text{ZPE}} + \Delta H_{0 \rightarrow T} - T\Delta S$$

where ΔE denotes the change in electronic energy obtained from DFT, ΔE_{ZPE} , $\Delta H_{0 \rightarrow T}$ and ΔS are the changes of the zero-point energy, the enthalpy and entropy at standard conditions ($T=298$ K and at potential vs RHE). The methodology for handling the adsorption energy of nitrate was derived from Federico et al⁵.

S3 Supplementary figures

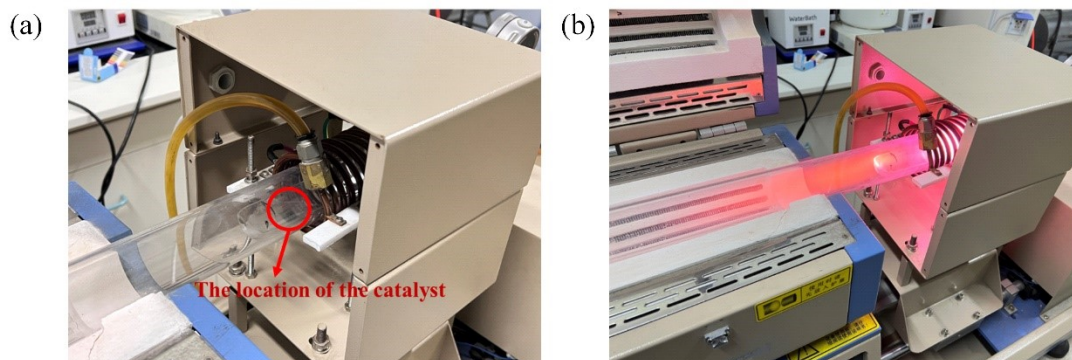


Fig. S1 a) Diagram of catalyst placement during discharge. b) Physical image of plasma discharge.

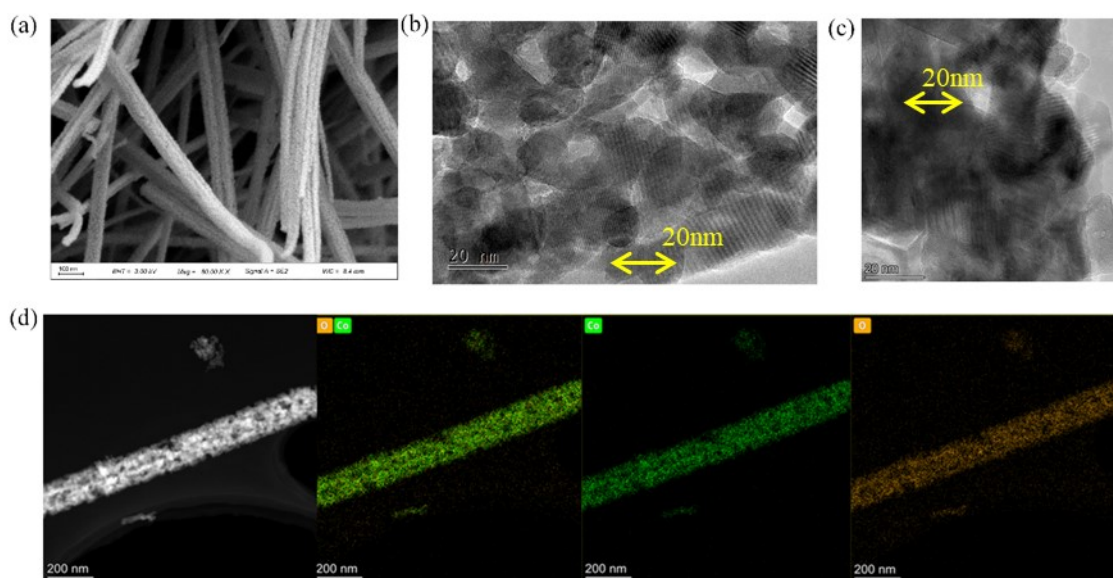


Fig. S2 a) SEM images and b) TEM images of V-Co₃O₄. c) TEM of Co₃O₄. d) Corresponding EDX elemental mapping images of Co and O for V-Co₃O₄.

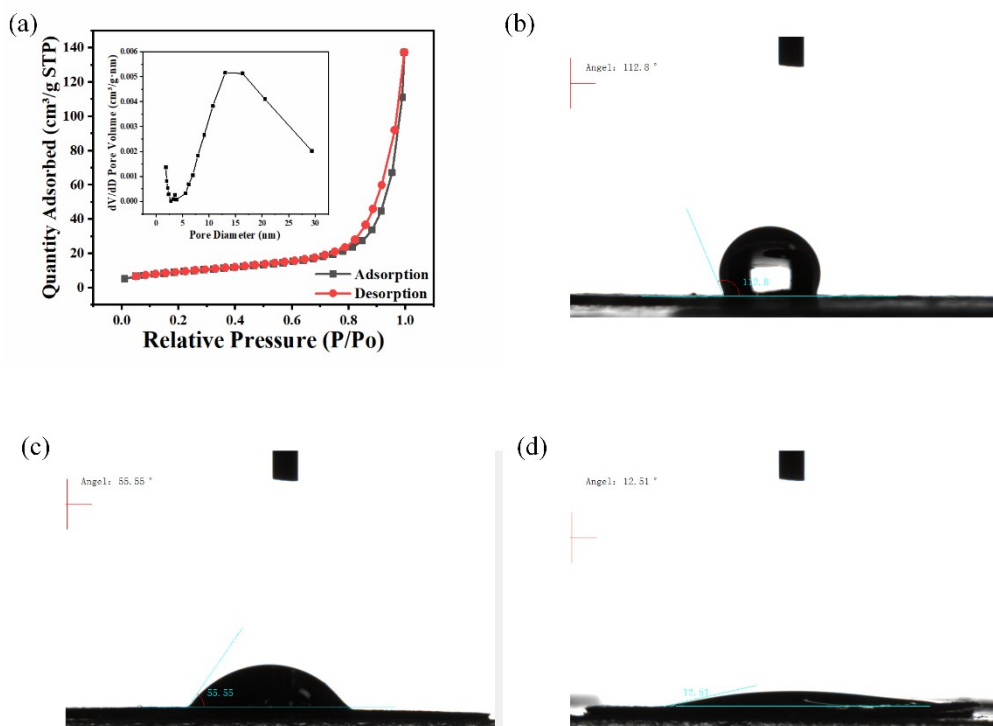


Fig. S3 a) N_2 sorption isotherms and pore-size distribution of Co_3O_4 . The contact angle with water of b) carbon cloth, c) Co_3O_4 , and d) $V-Co_3O_4$.

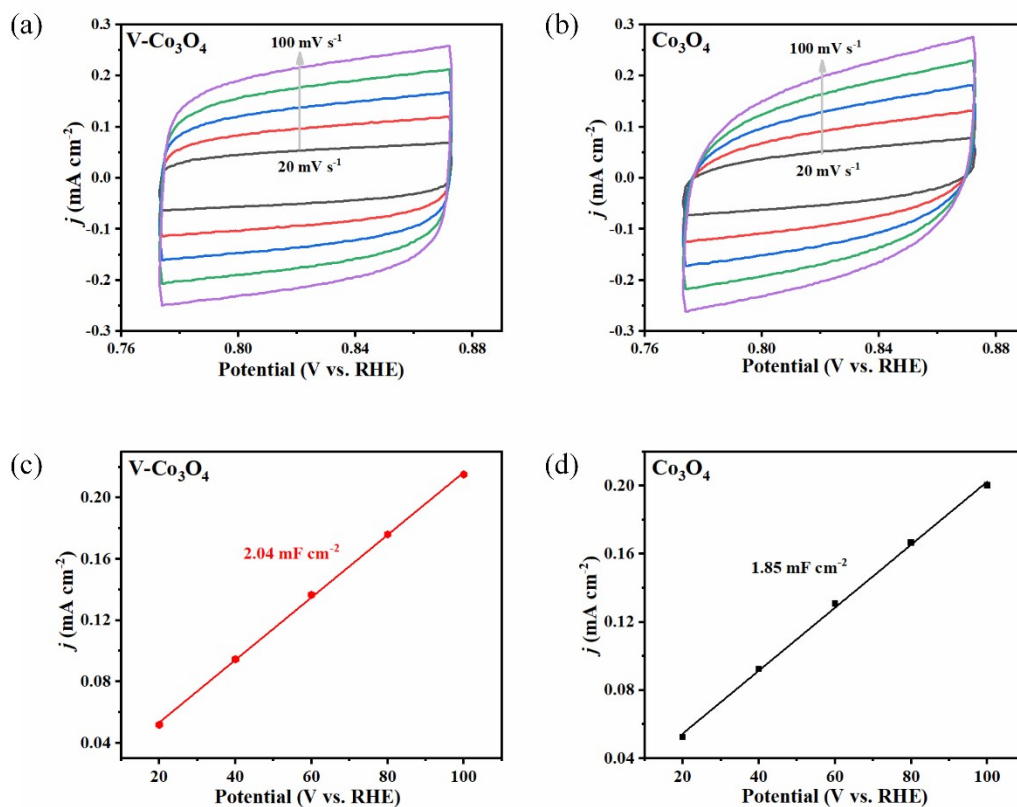


Fig. S4 CV curves for a) $V-Co_3O_4$, b) Co_3O_4 in the region of 0.77–0.87 V vs. RHE with various scan rates. Fitting curve of ECSA for c) $V-Co_3O_4$ and d) Co_3O_4 .

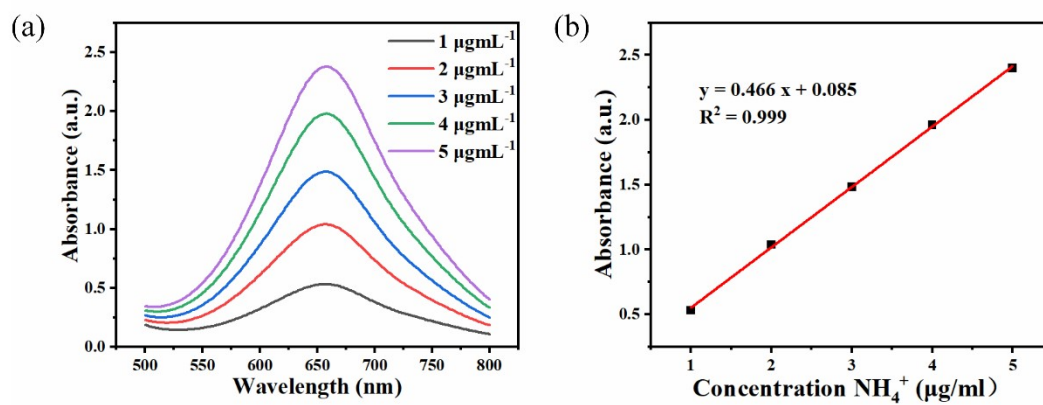


Fig. S5 a) UV spectra and b) calibration curve for determining NH_4^+ .

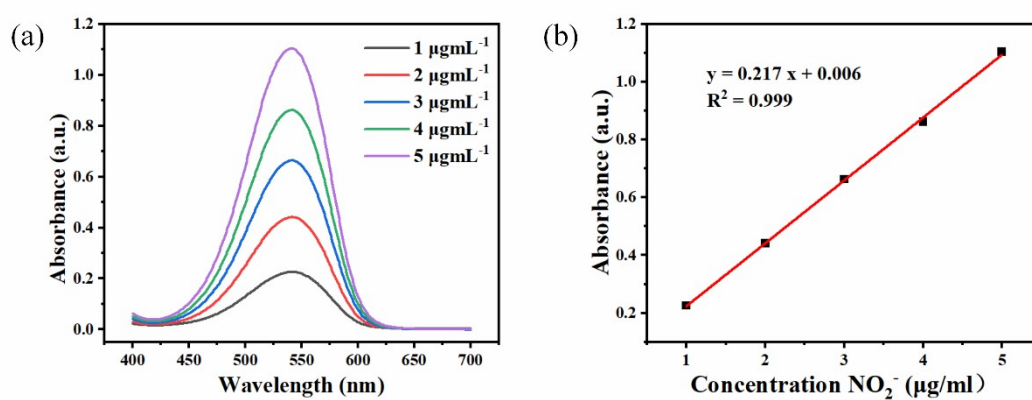


Fig. S6 a) UV spectra and b) calibration curve for determining NO_2^- .

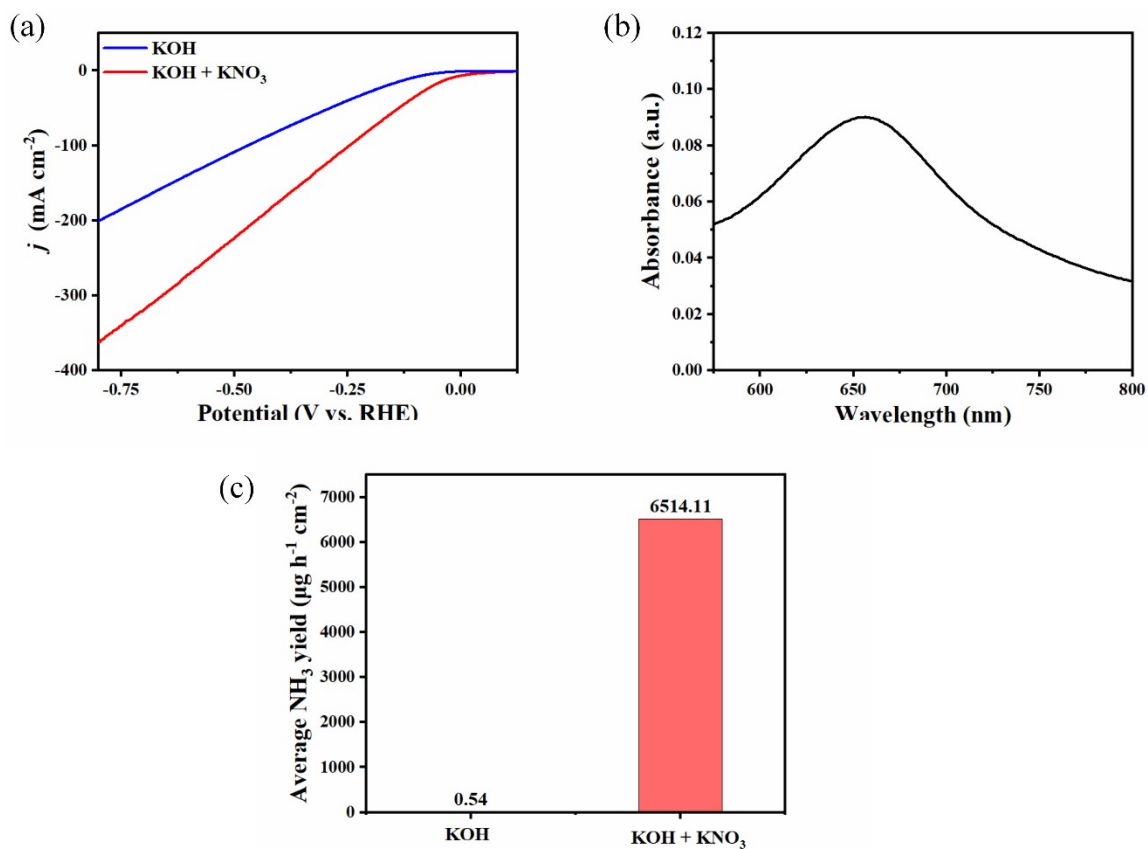


Fig. S7 a) LSV curves of V-Co₃O₄ in 1 M solution with/without KNO₃. b) UV-Vis extinction spectrum of an aqueous solution of 1 M KOH (blank) treated with indophenol blue method reagents. c) The NH₃ yield rate of V-Co₃O₄ in an aqueous solution of KOH (blank) and KOH / KNO₃.

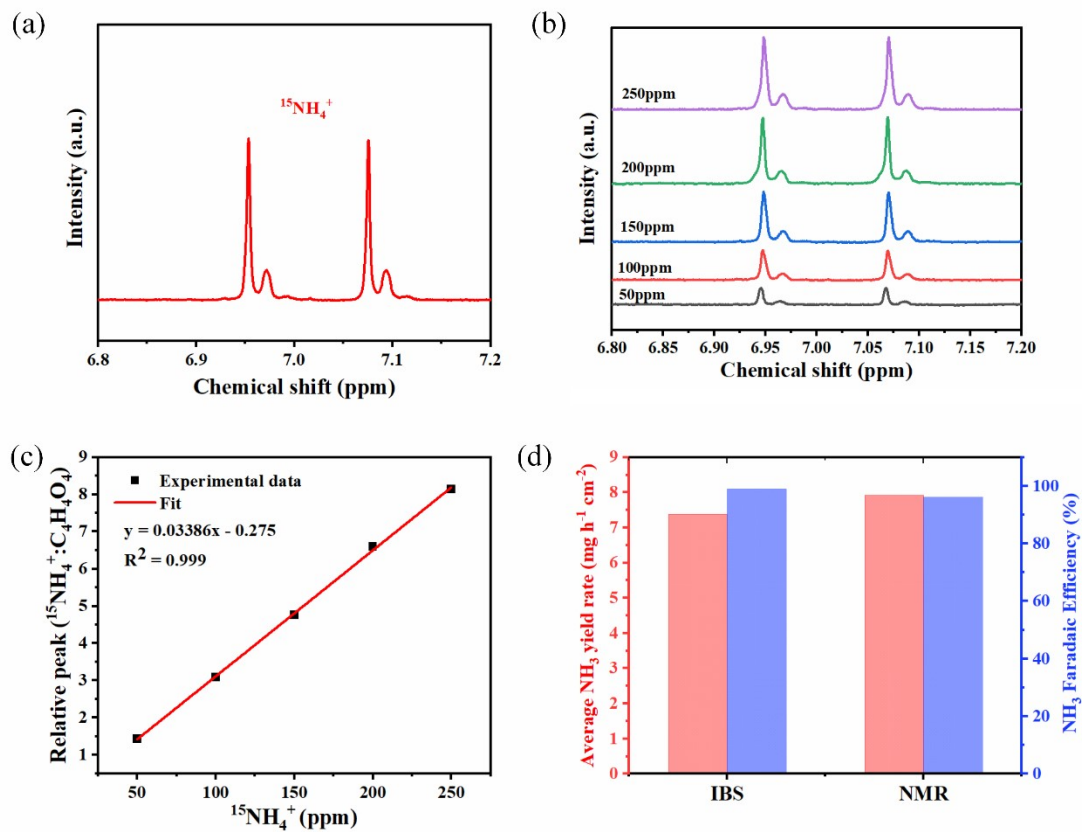


Fig S8 a) ^1H NMR tests of produced ammonia using K^{15}NO_3 as nitrogen sources. b) The standard curve of integral area ($^{15}\text{NH}_4^+ - ^{15}\text{N}/\text{C}_4\text{H}_4\text{O}_4$) against $^{15}\text{NH}_4^+ - ^{15}\text{N}$ concentration. c) ^1H NMR spectra of $^{15}\text{NH}_4^+ - ^{15}\text{N}$ with different concentration. d) The yield rate and FE of ammonia via IBS and ^1H NMR measurements.

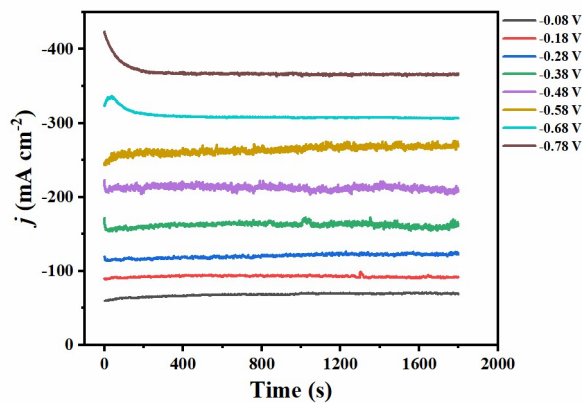


Fig. S9 Time-dependent current density curves of $\text{V-Co}_3\text{O}_4$ for the NO_3RR at different potentials.

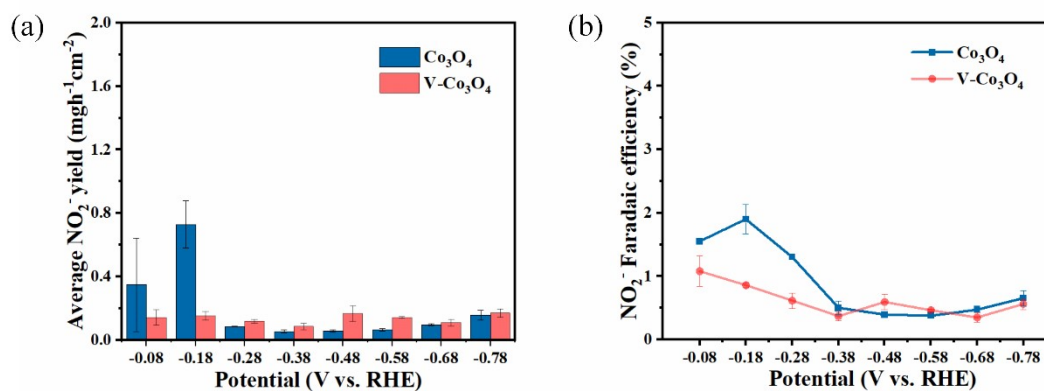


Fig. S10 a) NO_2^- yield and b) FE of Co_3O_4 .

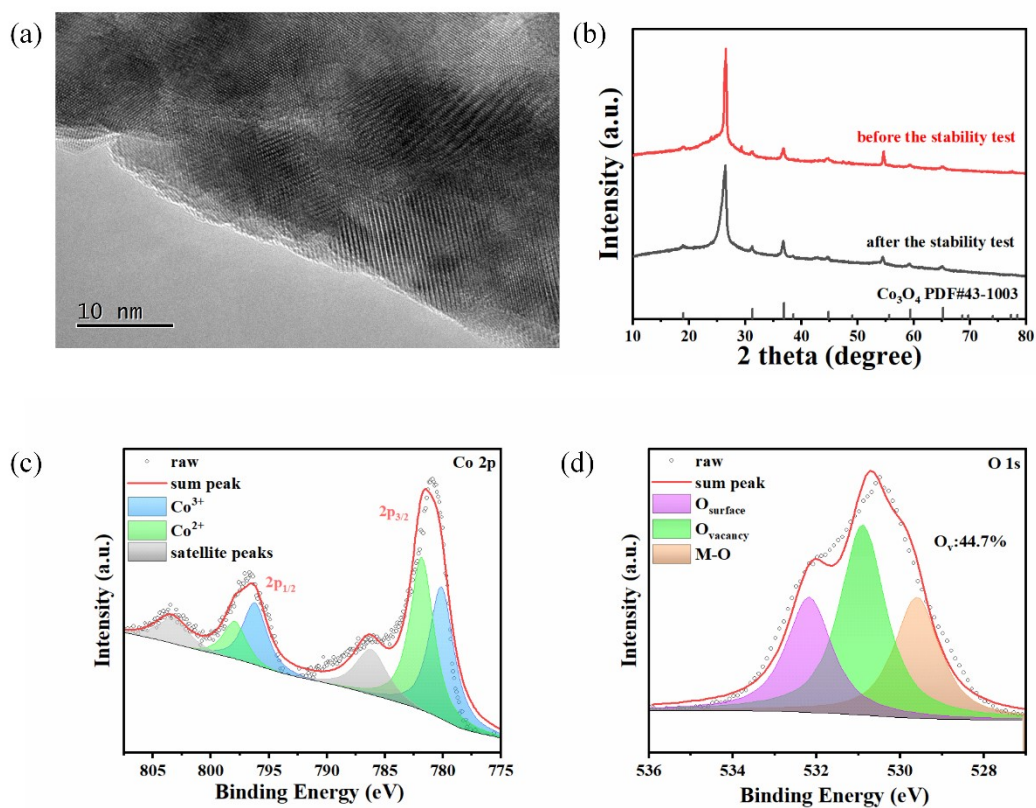


Fig S11 a) TEM and b) XRD of $\text{V-Co}_3\text{O}_4$ after stability test. XPS spectra of c) Co 2p and d) O 1s for $\text{V-Co}_3\text{O}_4$ after stability test.

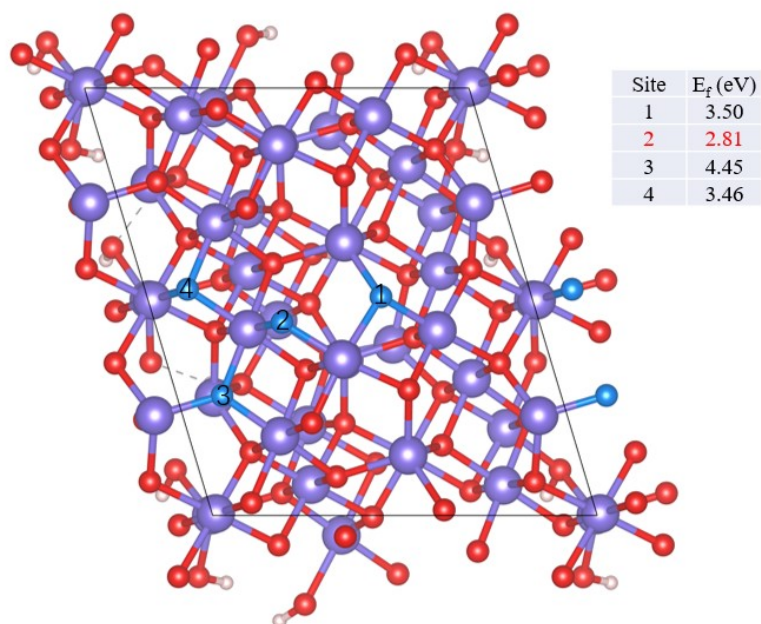


Fig S12 Diagrams of oxygen vacancies at different sites.

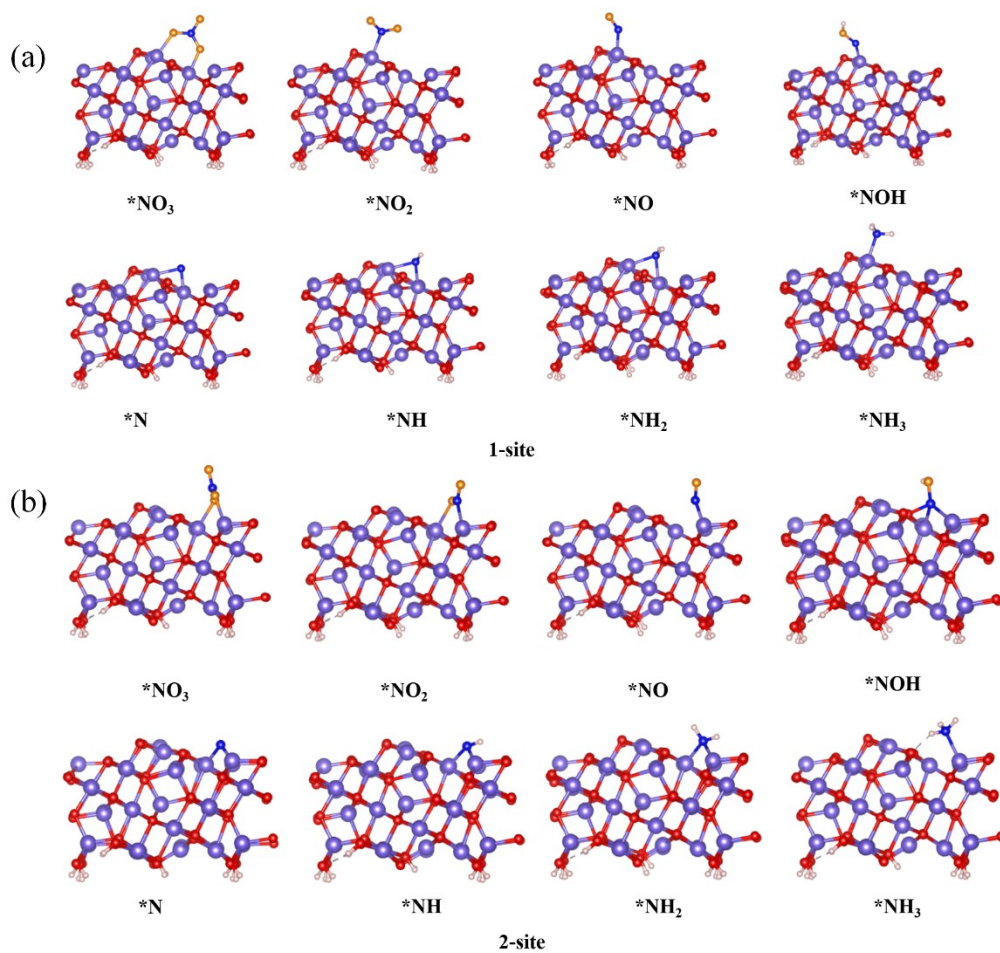


Fig. S13 Reaction diagram of different intermediates with a) V-Co₃O₄ and b) Co₃O₄.

Table S1 Comparison of catalytic performances for V-Co₃O₄ with other reported NO₃RR electrocatalysts

Catalyst	Electrolyte	NH ₃ yield @ Potential (μ mol h ⁻¹ cm ⁻² @ V vs. RHE)	FE @ Potential (% @ V vs. RHE)	Ref.
V-Co ₃ O ₄	1M KOH (0.1M NO ₃ ⁻)	27.45@-0.78	98.85@-0.08	This work
v _{Co} -Co ₃ O ₄	0.1M NaOH (0.1M NO ₃ ⁻)	8.8@-0.6	97.2@-0.4	6
Co ₃ O ₄ @CNF	0.1M NaOH (0.1M NO ₃ ⁻)	23.4 @-0.9	92.7@-0.9	7
CoO@NCNT/GP	0.1M NaOH (0.1M NO ₃ ⁻)	9.04@-0.6	93.8@-0.6	8
ZnCr ₂ O ₄	0.1M PBS (0.1M NO ₃ ⁻)	20.36@-1.2	90.21@-1.2	9
Fe-cyano-R NSs	1M KOH (0.1M NO ₃ ⁻)	21.1@-0.5	90@-0.5	10
Co@TiO ₂ /TP	0.1M PBS (0.1M NO ₃ ⁻)	13.6@-0.7	96.7@-1.0	11
B-doped MoS ₂	0.5M Na ₂ SO ₄ (0.1M NO ₃ ⁻)	10.8@-0.7	92.3@-0.7	12
VO-Co ₃ O ₄ /CC	0.1M NaOH (0.1M NO ₃ ⁻)	12.16@-0.5	96.9@-0.5	13
Co ₃ O ₄ /CC	0.1M NaOH (0.1M NO ₃ ⁻)	4.93@-0.5	56.9@-0.5	
FeCo ₂ O ₄	0.1M NaOH (20mM NO ₃ ⁻)	6.75@-0.7	95.9@-0.5	14
Co ₃ O ₄ @TiO ₂ /TP	0.1M NaOH (0.1M NO ₃ ⁻)	14.87@-0.9	93.1@-0.7	15
CoPc_RGO 1D-2D	0.1M K ₂ SO ₄ (200ppmM NO ₃ ⁻)	0.059@-0.2	95.12@-0.2	16
Co ₂ B@Co ₃ O ₄ /TM	0.1M PBS (0.1M NO ₃ ⁻)	8.57@-1.0	97@-0.7	17
P-FeCo ₂ O ₄ @CC	0.1M KOH (50mM NO ₃ ⁻)	4.2@-0.6	99.78@-0.4	18
S-Co ₃ O ₄	0.1M Na ₂ SO ₄ (0.1M NO ₃ ⁻)	2.96@-0.6	89.9@-0.6	19
NTCDA-LIG	0.1M NaOH (0.1M NO ₃ ⁻)	2.46@-0.94	83.7@-0.94	20
Fe ₃ O ₄	0.1M NaOH (0.1M NO ₃ ⁻)	1.01@-0.5	91.5@-0.5	21
Cu/Cu ₂ O@C	0.1M KOH (0.1M NO ₃ ⁻)	2.7@-0.6	76.97@-0.6	22

S4 Reference

- 1 G. Kresse and J. Furthmüller, *Phys. Rev. B*, 1996, **54**, 11169–11186.
- 2 P. E. Blöchl, C. J. Först and J. Schimpl, *Bull. Mater. Sci.*, 2003, **26**, 33–41.
- 3 D. J. Chadi, *Phys. Rev. B*, 1977, **16**, 1746–1747.
- 4 S. Grimme, J. Antony, S. Ehrlich and H. Krieg, *J. Chem. Phys.*, 2010, **132**, 154104.
- 5 F. Calle-Vallejo, M. Huang, J. B. Henry, M. T. M. Koper and A. S. Bandarenka, *Phys. Chem. Chem. Phys.*, 2013, **15**, 3196–3202.
- 6 Z. Deng, C. Ma, Z. Li, Y. Luo, L. Zhang, S. Sun, Q. Liu, J. Du, Q. Lu, B. Zheng and X. Sun, *ACS Appl. Mater. Interfaces*, 2022, **14**, 46595–46602.
- 7 L. Zhong, Q. Chen, H. Yin, J. S. Chen, K. Dong, S. Sun, J. Liu, H. Xian and T. Li, *Chem. Commun.*, 2023, **59**, 8973–8976.
- 8 Q. Chen, J. Liang, L. Yue, Y. Luo, Q. Liu, N. Li, A. A. Alshehri, T. Li, H. Guo and X. Sun, *Chem. Commun.*, 2022, **58**, 5901–5904.
- 9 S. Dong, A. Niu, K. Wang, P. Hu, H. Guo, S. Sun, Y. Luo, Q. Liu, X. Sun and T. Li, *Appl. Catal. B Environ.*, 2023, **333**, 122772.
- 10 Z. Fang, Z. Jin, S. Tang, P. Li, P. Wu and G. Yu, *ACS Nano*, 2022, **16**, 1072–1081.
- 11 X. Fan, D. Zhao, Z. Deng, L. Zhang, J. Li, Z. Li, S. Sun, Y. Luo, D. Zheng, Y. Wang, B. Ying, J. Zhang, A. A. Alshehri, Y. Lin, C. Tang, X. Sun and Y. Zheng, *Small*, 2023, **19**, 2208036.
- 12 Y. Luo, K. Chen, P. Shen, X. Li, X. Li, Y. Li and K. Chu, *J. Colloid Interface Sci.*, 2023, **629**, 950–957.
- 13 X. Xu, L. Hu, Z. Li, L. Xie, S. Sun, L. Zhang, J. Li, Y. Luo, X. Yan, M. S. Hamdy, Q. Kong, X. Sun and Q. Liu, *Sustain. Energy Fuels*, 2022, **6**, 4130–4136.
- 14 J. Li, D. Zhao, L. Zhang, L. Yue, Y. Luo, Q. Liu, N. Li, A. A. Alshehri, M. S. Hamdy, Q. Li and X. Sun, *Chem. Commun.*, 2022, **58**, 4480–4483.
- 15 X. Fan, C. Ma, D. Zhao, Z. Deng, L. Zhang, Y. Wang, Y. Luo, D. Zheng, T. Li, J. Zhang, S. Sun, Q. Lu and X. Sun, *J. Colloid Interface Sci.*, 2023, **630**, 714–720.
- 16 S. Paul, S. Sarkar, A. Adalder, S. Kapse, R. Thapa and U. K. Ghorai, *ACS Sustain. Chem. Eng.*, 2023, **11**, 6191–6200.
- 17 L. Xie, S. Sun, L. Hu, J. Chen, J. Li, L. Ouyang, Y. Luo, A. A. Alshehri, Q. Kong, Q. Liu and X. Sun, *ACS Appl. Mater. Interfaces*, 2022, **14**, 49650–49657.
- 18 T. Zhao, X. Li, J. Hu, J. Zhou, X. Jia and G. Hu, *J. Environ. Chem. Eng.*, 2023, **11**, 110122.
- 19 Z. Niu, S. Fan, X. Li, J. Yang, J. Wang, Y. Tao and G. Chen, *Chem. Eng. J.*, 2023, **451**, 138890.
- 20 L. Cheng, T. Ma, B. Zhang, L. Huang, W. Guo, F. Hu, H. Zhu, Z. Wang, T. Zheng, D.-T. Yang, C.-K. Siu, Q. Liu, Y. Ren, C. Xia, B. Z. Tang and R. Ye, *ACS Catal.*, 2022, **12**, 11639–11650.
- 21 X. Fan, L. Xie, J. Liang, Y. Ren, L. Zhang, L. Yue, T. Li, Y. Luo, N. Li, B. Tang, Y. Liu, S. Gao, A. A. Alshehri, Q. Liu, Q. Kong and X. Sun, *Nano Res.*, 2022, **15**, 3050–3055.
- 22 G. Li, S. Xue, H. Zhu, Z. Liang, F. Zhao, Q. Hua, X. Ren, W. Xiong, L. Gao and A. Liu, *Ionics*, 2023, **29**, 2515–2522.